Cybernetics of Vision Systems: Towards an Understanding of Putative Functions of the Outer Retina

Tomás Maul, Andrzej Bargiela and Lee Jung Ren
School of Computer Science
University of Nottingham Malaysia Campus
Malaysia
Telephone: 00-6-03-89248232

***Abstract*—The retina still poses many structural and computational questions. Structurally, for example, it is not yet clear how many distinct horizontal cell (HC) types the primate retina contains and what the exact patterns of connections between photoreceptors (PRs) and HCs consist of. Computationally, it is not yet clear, for instance, what functions are present and how they are being implemented. This paper proposes a model (a Linear Recurrent Neural Network defined by 31 parameters) of the outer retina and an optimization methodology that hopes to shed some light on these questions. The paper shows that a simplified model of the outer retina can implement several low-level visual functions involving the modulation of noise, brightness, contrast, saturation and even colour. The results demonstrate that contrast control functions can be implemented with a minimum of two HC types and that spectral specificity between PRs and HCs is a common and important feature. It is also shown that several different spectrally specific patterns can emerge in order to implement the same function. One interesting micro-circuit that naturally emerged from our experiments involves non-blurry denoising via inter-chromatic gap junctions and compensatory re-saturation via HC circuits, a strategy we hypothesize exists in some biological retinae.**

***Index Terms*—Outer retina, cones, horizontal cells, image processing, denoising, contrast enhancement.**

I. Introduction

A great deal is known about the structure and function of the primate retina. However, some crucial questions remain unanswered. In this paper we extend and elaborate on the artificial neural network model introduced in [1], to provide clues regarding the structure and function of the outer retina (i.e. the Outer Plexiform Layer and its related cells) from the standpoint of cybernetics. For example, there is still a debate on whether there are three or only two different types of horizontal cells (HCs) [2] [3]. Another important structural question pertains to the connectivity patterns between photoreceptors and horizontal cells. In particular, there is still some debate on whether there is spectral specificity in these connection patterns (e.g. does a particular HC type have more connections with green cones compared to connections with red cones?). The answers to these questions are desirable not only because of their impact on neuroanatomical knowledge, but also because of how much light they can potentially shed on functional questions pertaining to the retina. The precise number and nature of functions is still a matter of debate. Candidate functions, which are non-mutually exclusive, include the modulation of brightness, contrast, noise, saturation and colour, and the mediation of center-surround phenomena and possibly even chromatic opponency. Even for outer retina functions which are quite well established such as contrast gain control (CGC), there is still the question of how exactly they are mediated by the circuitry and electrophysiology of the outer retina. Although the phenomenon of CGC has clearly been identified at the level of bipolar cells (BC) [4], there is no consensus on how exactly the phenomenon is generated. Apart from functional questions, there is also plenty of scope for increasing our understanding of the representational and coding solutions of the retina [5].

Questions pertaining to low-level visual functions are not the exclusive domain of Computational Neuroscience and indeed could be seen as key pursuits of Cybernetics as an interdisciplinary study of the structure of regulatory systems. On the applied side, and in particular in fields such as Image Processing, plenty of work is still being done in order to improve the accuracy and speed of algorithms involved in image enhancement (e.g. denoising, sharpening and colour correction). Solutions based on Neural Computation tend to automatically provide algorithms with useful properties such as graceful degradation, robustness, generalization, adaptability and parallelizability. In view of the fact that the area of image enhancement has not yet reached full maturity and our knowledge about biological neural systems is still in its infancy, this Natural Computation effort, that involves transferring solutions (or inspiration) from nature to applied algorithms has not yet reached a state of saturation. This paper aims to not only shed some light on questions pertaining to the outer retina, but also to provide the basis for new image enhancement algorithms based on the structure and function of the retina. Refer to [6] for a useful review of the application of Artificial Neural Networks to different Image Processing problems.

The retina consists of several main layers, i.e.: outer nuclear layer, outer plexiform layer, inner nuclear layer, inner plexi-

form layer and ganglion cell layer. Most connections between cells can be found in the outer and inner plexiform layers. In the nuclear and ganglion cell layers several main categories of cells can be found, i.e.: photoreceptors, horizontal cells, bipolar cells, amacrine cells and ganglion cells. Each one of these categories can be subdivided into several subcategories differentiated in terms of factors such as morphology, electrophysiology and connectivity. If we consider cell subcategories, all in all the retina consists of approximately 55 distinct types of cells [7]. Most retinal cells communicate with graded potentials, with the exception of retinal ganglion cells which communicate via action-potentials. This makes the retina an interesting and useful subject of study in order to understand "analogue to digital conversions" in the biological domain. As was mentioned earlier, in this paper, we focus on the outer retina, and in particular on cones, horizontal cells and their connectivity patterns.

As mentioned above, several important debates in the Outer Plexiform Layer (OPL) literature include: 1) whether there is spectral specificity in the connections between photoreceptors (PRs) and horizontal cells (HCs), 2) how many distinct types of HCs exist and 3) what the function of HCs are (e.g. luminance gain control [8], contrast gain control [4], center-surround receptive fields [9] and chromatic opponency [10]).

Evidence and arguments in favor of the view that HCs do not connect preferentially to cones of particular wavelengths can be found in [11]. It is argued for instance that the fact that some HC types tend to exhibit no connections with blue cones, is a reflection of the lower proportion (approximately 10% on average) of blue cones in the retina [12], the fact these blue cones are spread out in a regular pattern [13], and the small dendritic fields of those HCs. Evidence in favour of PR-HC spectral specificity can be found in [14] and [3]. Some authors have taken care to demonstrate that this spectral specificity does not imply that HCs mediate the chromatic opponency phenomena observed in retinal ganglion cells (RGCs) [3]. Moreover, even amongst those that believe in PR-HC spectral specificity, there is lack of certainty as to what are the exact proportions of connections between the different cone and HC types. Our OPL model allows us to control these proportions and thus to test different possibilities and to hopefully shed some light on these uncertainties.

According to [3], and consistent with other mammalian retinae [15], the primate OPL seems to consist of only two HC types. However, according to [14], the primate OPL appears to consist of 3 different HC types (H1, H2 and H3). The H1 cell appears to have sparse connections with blue cones, whereas H2 seems to contact all cones (with a relatively large blue proportion), the dendritic tree of H3 seems to avoid blue cones completely and the axonic tree of H3 seems to connect to blue cones exclusively. Going back to [3], it is argued that the distinctive morphological features of the putative H3 cell is captured by the natural morphological variation of the H2 cell. For the macaque retina, the general consensus is that there are two HC types [16], i.e.: H1 and H2. The dendrites of H1 cells contact most cones in their dendritic fields, with a relatively lower preference for S-cones, while the axons of H1 cells contact rods. The dendrites of H2 cells contact most cones within their fields with a relative preference for S-cones while the axons of H2 cells appear to contact only S-cones [17]. If we assume that the axonal terminals of both H1 and H2 cells are electrotonically isolated (which is not confirmed for the H2 case) then, at least in the macaque, we have four effective HC types (three involving cones). Computational studies of the functional consequences of different numbers and natures of HC types should be capable of evaluating the relative merits of the various positions in this debate. The poignant morphological differences between the axonal processes of H1 and H2 types, with their computational repercussions, might be explained via future detailed models of these cell types.

Although, so far, there seems to be no high-profile concerted effort to build a very detailed model of the biological retina, there is a sizable number of relatively simplified models scattered throughout the literature, with differing levels of detail and sources of motivation, which consist of biological, software and hardware goals. A good example of a biologically oriented model consists of [18], where the prime objective is to build a simplified network that can replicate empirical data. The underlying motivation common to both software and hardware oriented models is the development of image processing solutions. In the software case, the developed algorithms may run on different computing platforms (e.g. [19]), whereas in the hardware case [20], special purpose circuits emulating the retina are developed in order to obtain extremely efficient and robust image processing functions (with possible medical repercussions).

Other biologically oriented retinal modeling studies include [21], [22] and [23]. The first paper reports a model of the spatiotemporal processing properties of primate cones and horizontal cells. In the second paper a retinal model was built to demonstrate the interaction between sensitivity regulation and temporal dynamics. The third paper consists of an early attempt to accurately model the OPL. Although the above models have contributed significantly to our understanding of the retina, to the best of our knowledge, there are still no models that attempt to parameterize the potential spectral specificities of PR-HC connectivity. This parameterization is indeed included in our model, which thus allows us to begin to tackle some of the unresolved issues pertaining to OPL structure and function.

Our early efforts to model the retina in greater detail are part of a broader framework to accurately model the early visual system (e.g. retina, superior colliculus, lateral geniculate nucleus and visual cortical area V1). In order to guide us in this ambitious task we have equipped ourselves with two general philosophies, i.e.: Neuroalgorithmics and incremental modeling. Neuroalgorithmics can be seen as subfield that lies at the intersection between Computational Neuroscience and Natural Computation. It is thus concerned with both understanding biological neural systems (i.e. reverse engineering) and extracting and improving natural algorithms to be applied to real-world problems (i.e. re-engineering). It is hoped that this dual

concern will motivate a new framework and methodologies for tackling open problems such as those mentioned above. The viewpoint of incremental modeling corresponds to a relatively purist bottom-up approach, whereby earlier processing stages need to be modeled before later ones, because of input/output dependencies. Of course, where layers depend on feedback from higher regions, temporary approximations are required. Since the lowest level of any computational system that interacts with the environment consists of signals, sensors and their connections, and our interest lies in early vision, our initial focus is on light and the outer retina.

Because of the numbers of cells and connections involved, detailed simulations of the retina can generally be considered large-scale models, and therefore, it was not practical at this early stage to use compartmental models. Moreover, the types of scientific questions pursued in this work (e.g. spectral specificity of PR-HC connections) do not require modeling at this detailed level. Thus, it was sufficient to model the outer retina using a linear recurrent neural network (LRNN) [24], fully specified by a set of 31 parameters. These parameters allow for several LRNN structural features to be controlled such as the dimensions of HC dendritic fields and the proportions of connections between HC types and cones of different wavelengths. According to [25], in most modeling efforts either the connectivity between cells is not fully known or the system's input/output patterns are not fully understood. In the case of the outer retina (as with probably all other sub-systems in the early visual system), we have incomplete knowledge of both connectivity and input/output patterns. The flexible parameterization of our LRNN provides us with the opportunity to fill in the connectivity gap, whereas optimization experiments with cost functions involving different low-level visual functions allow us to begin unravelling the input/output patterns of the outer retina.

The following section outlines the proposed method of investigation in some detail. In particular it specifies the nature of the model and briefly describes the optimization methodology used for exploring the functional capabilities of the network. Section III describes the main results that the model has yielded thus far and section IV discusses the implications of these results in relation to the scientific questions and engineering goals outlined in the introduction.

II. Methods

A. The Model

Our model is essentially an OPL-inspired LRNN. As with most modeling exercises several decisions were made as to what details to include in the model. Because of our focal interest in the chemical and electrical connectivity of OPL cells and their functional consequences we chose to include the following main aspects:

- Different types of cone photoreceptor (PR) cells.
- Gap junctions (GJ) with different weights between different PRs.
- Excitatory feedforward and inhibitory feedback connections between PRs and HCs.
- Different types of HCs (with different dendritic tree radii and other properties).
- Differently weighted GJs between different HC types.
- Variable proportions of connections between different PR and HC types.

Some of the biological details currently abstracted out by the model include ionic currents, rod photoreceptors, variable cell densities and cell properties that vary according to eccentricity (e.g. HC dendritic tree radius). One significant simplification pertains to the representation of light in terms of pixels, and the assignment of three cones per pixel. This simplification ignores facts such: 1) S-cones represent only about 10% of the cone population, 2) the fovea is practically devoid of S-cones and 3) overall, there are about 2 to 4 times more L-cones than there are M-cones.

The specific structure and basic temporal behaviour of different instantiations of the LRNN model are fully specified by a set of 31 parameters (Table I). Through these parameters we can define and test instances of the model that are differentiated based on different connectivity patterns between PRs and HCs, different dendritic tree radii, and so on. Table I lists down and briefly describes each one of the model parameters. The notation HC_n refers to an HC type indexed by n. A *solution*, or a model instance, consists of a vector defined by the values of each one of these 31 parameters. For representational consistency and in order to simplify the optimization process, every single parameter is normalized to the range $[0, 1]$. For parameters that ultimately need to be represented by a natural number we include an extra parameter that defines it's maximum natural value. In these cases, the final parameter value is computed via $r(p_i \times max_i)$ where r is the rounding function, p_i represents the value of the parameter with index i and max_i specifies the maximum (natural) value of the attribute associated to parameter p_i. The only model attributes that require this scaling step consist of: number of iterations, HC input radius and HC output radius. All the experiments reported in this paper utilized the following maximum values:

- Number of iterations: 2.
- HC input radius: 3.
- HC output radius: 3.

Figures 1, 2 and 3 consist of diagrammatic representations of the OPL model. The main parameterizations adopted at the PR layer are depicted in Fig. 1. In particular notice the parameterization of light (P1), self-regulation (P2), GJs between PRs in the same position but of different chromaticities (P3), GJs between PRs from different positions but the same chromaticities (P4) and GJs between PRs from both different positions and different chromaticities (P5).

Figure 2 depicts parameters that determine the connectivity between the PR layer and a horizontal cell HC_1. The depicted connectivity and parameterization patterns generalize directly to cases involving HC_2 and HC_3 cells. The PR layer is represented in 1D rather than 2D in order to simplify the illustration. Notice how input from the PR layer comes from

TABLE I
LRNN PARAMETER DESCRIPTIONS.

P1	Weight of the influence of light on cones
P2	Weight of a cone's influence on itself
P3	Cone GJ weight: intra-positional and inter-chromatic
P4	Cone GJ weight: inter-positional and intra-chromatic
P5	Cone GJ weight: inter-positional and inter-chromatic
P6	Radius of input from the PR layer onto HC1 cells
P7	Radius of output from HC1 cells to the PR layer
P8	Proportion of synapses from red cones onto HC1 cells
P9	Proportion of synapses from green cones onto HC1 cells
P10	Proportion of synapses from blue cones onto HC1 cells
P11	Relative connection weights from PRs onto HC1 cells
P12	Relative connection weights from HC1 cells onto PRs
P13	Radius of input from the PR layer onto HC2 cells
P14	Radius of output from HC2 cells to the PR layer
P15	Proportion of synapses from red cones onto HC2 cells
P16	Proportion of synapses from green cones onto HC2 cells
P17	Proportion of synapses from blue cones onto HC2 cells
P18	Relative connection weights from PRs onto HC2 cells
P19	Relative connection weights from HC2 cells onto PRs
P20	Radius of input from the PR layer onto HC3 cells
P21	Radius of output from HC3 cells to the PR layer
P22	Proportion of synapses from red cones onto HC3 cells
P23	Proportion of synapses from green cones onto HC3 cells
P24	Proportion of synapses from blue cones onto HC3 cells
P25	Relative connection weights from PRs onto HC3 cells
P26	Relative connection weights from HC3 cells onto PRs
P27	Weight of an HC's influence on itself
P28	HC GJ weight: same position, different HC type
P29	HC GJ weight: different position, same HC type
P30	HC GJ weight: different position, different HC type
P31	Number of iterations

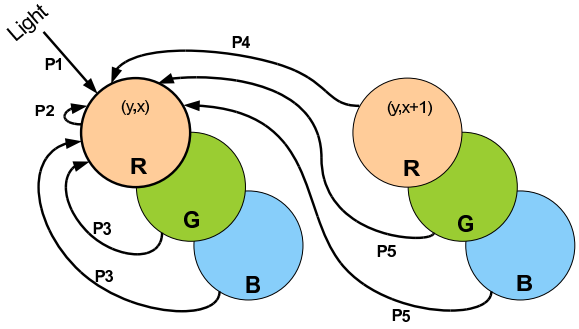

Fig. 1. Photoreceptor parameters.

central regions whereas output to the PR layer is sent to surrounding regions. The PR layer on the top consists of long-wavelength (red) cones, whereas the layer on the right consists of medium-wavelength (green) cones and the one at the bottom corresponds to short-wavelength (blue) cones. The input radius is governed by parameter P6, whereas the output radius is determined by parameter P7. Parameters P11 and

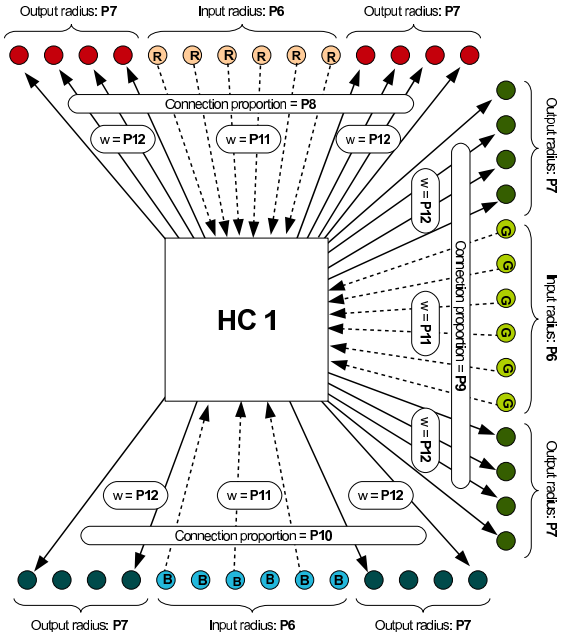

Fig. 2. PR-HC connectivity parameters.

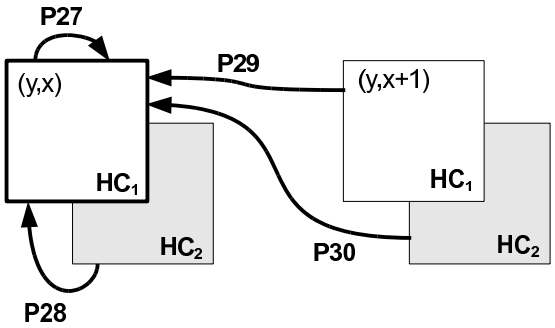

Fig. 3. Horizontal cell parameters.

P12 determine the weights of input connections from HC to PR cells and HC to PR cells respectively. The proportions of connections between cones of specific wavelengths and HC_1 cells are defined by parameters P8, P9 and P10 for red, green and blue cones respectively. Notice how, in the diagram, the proportion of connections between blue cones and the HC_1 cell is approximately half of the proportions involving red and green cones.

Figure 3 depicts two different HC types and their relevant parameters. Parameter P27 conditions the influence that HC_1 cells have on themselves. The influence that HC cells have via GJs on other HC cells of a different type and in the same position is determined by P28. Parameter P29 specifies the GJ strength of HCs of the same type and at different positions. For HCs in different positions and of different types, the corresponding GJ strength is specified by P30.

Equation 1 encapsulates the update rule for the PR layer. As the equation shows, the main inputs to any PR cell originate

from light, the cell itself and nearby PR and HC cells:

$$b_{ip}^{t+1} = w_1 a_{ip}^t + w_2 b_{ip}^t + w_3 \sum_{j \neq i} b_{jp}^t + w_4 \sum_{p' \in n(p)} b_{ip'}^t + \\ + w_5 \sum_{\substack{j \neq i \\ p' \in n(p)}} b_{jp'}^t - \sum_{h \in H} w_h \left(\sum_{(hp') \in v(ip)} c_{hp'}^t \right) \quad (1)$$

where a represents light intensity in the range $[0, 1]$ (for a particular chromaticity and position, indexed by i and p respectively), b represents PR cell activity (for a particular type indexed by i or j and a particular position indexed by p or p'), c represents HC cell activity (for a particular type and position, indexed by h and p' respectively) and t denotes iteration number. Note that the term *activity* does not directly represent membrane potential, although it does plausibly reflect relative potentials. The set of neighbours $n(p)$ is defined in Equation 2 while the set of connections $v(ip)$ is defined in Equation 3. Influence weights are denoted by w_i where the subscript refers to the corresponding parameter i in Table I. The weight w_h represents the influence of HC cells of type h on PR cells. Although weights are based on their corresponding parameters, actual weights are normalized by the total sum of weights used in a particular cell update, which means that a non-linear saturating function is not required in order to keep activations bounded.

$$n(p) = \{p' \mid p' \neq p \wedge d(p'_x, p_x) \leq r \wedge d(p'_y, p_y) \leq r\} \quad (2)$$

where $d(p'_x, p_x)$ represents the distance between positions p and p' along the x-axis and r represents the *radius* of GJ influence.

$$v(ip) = \{(h, p') \mid con(PR_{ip}, HC_{hp'}) \equiv 1\} \quad (3)$$

where $con(c_1, c_2) \equiv 1$ denotes that a feedforward connection exists from cell c_1 to cell c_2.

Equation 4 encapsulates the update rule for the HC layer:

$$c_{hp}^{t+1} = w_{h'} \left(\sum_{(ip') \in v(hp)} b_{ip'}^t \right) + w_{27} c_{hp}^t + w_{28} \sum_{k \neq h} c_{kp}^t + \\ + w_{29} \sum_{p' \in n(p)} c_{hp'}^t + w_{30} \sum_{\substack{k \neq h \\ p' \in n(p)}} c_{kp'}^t \quad (4)$$

where b, c, t, i, p, p', w_i and $n(p)$ are defined as before, k represents HC type, $v(hp)$ is defined in Equation 5 and $w_{h'}$ represents the weighted influence of PR cells on HC cells of type h.

$$v(hp) = \{(i, p') \mid con(PR_{ip'}, HC_{hp}) \equiv 1\} \quad (5)$$

The connectivity between PRs and HCs is defined by different dendritic tree input/output radii, synaptic connections with different spectral proportions and different input/output synaptic weights. (refer to Table I: P6 to P26). In order to increase the efficiency of simulations we assume that connectivity patterns are consistent throughout the whole spatial domain of the modeled OPL, and therefore we make use of connectivity templates. Each HC type is associated with a different connectivity template, which is repeatedly used for all HCs belonging to that type.

In order to initialize the network a simple sequential activation process is used. The PR layer is initialized by allowing *light* (i.e. the input RGB image), which is normalized to the range $[0, 1]$, to be copied to the PR layer. The HC layer is initialized based on the activations of PRs and the connectivity patterns between the PR and HC layers, whilst ignoring the effects of HC GJs.

After initialization, the network is run for one or more iterations (depending on P31 and the parameter specifying the maximum number of iterations allowed).

B. Optimization

As was mentioned earlier, different instantiations of our OPL model are specified via different sets of parameter values, or different solution vectors. In order to explore plausible structural and functional OPL characteristics we subjected the model to a battery of optimization experiments. Different sets of optimization experiments were defined by different visual functions involving the modulation of brightness (i.e. $\uparrow\downarrow$ brightness), contrast (i.e. $\uparrow\downarrow$ contrast), noise (i.e. $\downarrow$ noise), saturation (i.e. $\uparrow\downarrow$ saturation) and colour (e.g. $\uparrow\downarrow$ redness), where $\uparrow$ denotes an increase and $\downarrow$ denotes a decrease of the image property. In order to optimize the network vis-a-vis different visual functions, different cost functions were constructed involving different source and target images and an image comparison metric. If for instance, the objective is for the network to be optimized for contrast enhancement, then the corresponding cost function is constructed by taking a source image with moderate contrast, constructing a target image which is identical to the source except for enhanced contrast, and using an image similarity metric (e.g. mean absolute pixel differences). In this case, the cost is the distance between the processed image (i.e. PR layer at the last iteration) and the target image. In all optimization experiments image resolution was confined to 100×100. Note that, after optimizing the LRNN for a new visual function, the result is almost invariably a new set of parameters, and therefore a new network configuration.

Our optimization process belongs to the category of Global Stochastic Optimization (GSO) algorithms. In particular, we combined elements of Differential Evolution [26] and Genetic Algorithms [27] [28]. Table II lists the GSO's main parameters with typical settings. We start with an initial set of *ngSize* solutions which are ranked according to cost. This solution set is then expand via differential evolution (DE). In our implementation of DE, for every leader that is sufficiently different from the previously considered leader (as defined by *minDiffLL*), the first sufficiently different follower (as defined by *minDiffLF*) is found and then used to compute a velocity

TABLE II
GSO PARAMETERS.

Parameter	Setting	Comment
maxIter	100	Maximum number of iterations.
threshCost	0.1	Threshold solution cost.
ngSize	20	Size of each new generation.
percTrim	0.4	Percentage of solutions to trim.
minDiffLF	0.1	Min. dif. (leader & immediate-follower).
minDiffLL	0.3	Min. dif. (two consecutive leaders).
minDiffTrim	0.1	Min. dif. (trimmed solutions).
α	0.25	Differential Evolution rate.
gvAmplify	100	Amplification (for combined velocity).
mutRange	0.2	Mutation "intensity".
mutProb	0.5	Probability of mutation.

vector (i.e. $v = l - f$ where v, l and f correspond to *velocity*, *leader* and *follower* respectively), which is then multiplied by α and added to the leader to form a new solution. An additional solution is also generated by averaging all of the velocities computed in a particular DE round into a *combined velocity*, which is then multiplied by *gvAmplify* and added to the best solution of the original set. After DE, the costs of new solutions are evaluated and all solutions are again ranked.

Subsequent to this initialization phase, the GSO algorithm iterates until the current iteration exceeds *maxIter* or the current best cost is inferior to *threshCost*. Each iteration consists of trimming the current solution set, applying genetic algorithm (GA) operators and expanding this set via DE. The trimming function attempts to create a solution set whose size is determined by round(*percTrim* $\times$ *ngSize*) and consists of solutions which are sufficiently different from each other (as defined by *minDiffTrim*). Our simple implementation of a GA first estimates how many solutions need to be added to the trimmed set in order to create a set of *ngSize* solutions and then, for each new solution, randomly selects one of three possible actions: 1) mutate, 2) cross-over or 3) generate a random solution. The mutation operator randomly selects a solution from the trimmed set and then considers each parameter, which it mutates (with a probability of *mutProb*) using a mutational range of *mutRange*. The cross-over operator randomly selects two different solutions from the trimmed set and generates a new solution based on a random cross-over location and the original solutions. Following this, the new solution set is expanded via DE (as already described) and the new set is finally evaluated and ranked before moving onto the next GSO iteration.

Although our GSO is a hybrid algorithm, we don't expect any other commonly used GSOs to perform less effectively in the optimization problems reported in this paper.

III. RESULTS

Figure 4 demonstrates some of the processing capabilities of our OPL model. The bottom-row corresponds to the processed versions of the images in the top-row. Processed images are extracted from the PR layer after the last simulation iteration.

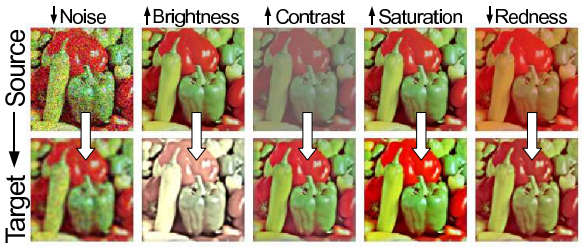

Fig. 4. Processing examples.

Since the PR layer consists of three cone types, the PR layer can be seen to consist of three sub-layers, one for each cone type. Information for each image colour channel (i.e. red, green and blue) is extracted from each corresponding PR sub-layer. Each column in Fig. 4 corresponds to a different visual function and therefore a different optimized network configuration. The functions depicted from left to right are: $\downarrow$ noise, $\uparrow$ brightness, $\uparrow$ contrast, $\uparrow$ saturation and $\downarrow$ redness.

Although each network is optimized using only one image, the resulting solutions seem to generalize well to new images. Table III demonstrates this generalization capability. Each network configuration (leftmost column), optimized in relation to a different visual function (and using only one image), was tested in relation to ten new images. The second column counting from the left, depicts the network's accuracy when confronted with new images. Accuracy is computed by taking the ratio of correctly processed images over the total number of test images. Assuming that we are testing the correctness of an $\uparrow$contrast network, and that we have been given a source image I_s and that the processing result is I_p, then the processing is deemed correct if $contrast(I_p) > contrast(I_s)$. The third column from the left depicts mean image measure (e.g. contrast) differences whereas the last column depicts the most significant difference.

Estimating noise based on single images is difficult partly because of the fact that pixel variations can be due to noise or natural causes such as pigmentation, texture, shape and light intensity [29]. Because we are interested in relative noise measures (i.e. image noise before and after processing), the average standard deviation of local patches is sufficient as a rough noise estimate (refer to [30] for adaptive noise estimation approaches based on the standard-deviation). Image brightness was measured by first converting images from the RGB to the HSV colour space and then computing the mean of all V values. Image saturation was measured by converting images from the RGB to the HSV space and then computing the mean of all S (i.e. saturation) values. Finally, redness was measured by averaging and normalizing red to green and red to blue ratios. Contrast was measured by averaging all ratios between local maxima and minima and normalizing by the largest possible ratio (i.e. 255):

$$\frac{1}{255\ n} \sum_{c \in I} \frac{max\left(R_c\right)}{min\left(R_c\right)} \tag{6}$$

TABLE III
SOME GENERALIZATION RESULTS.

Function	% Correct	Mean	Max.
↓ Noise	100	−3.04	−4.18
↑ Brightness	60	−0.02	0.04
↓ Brightness	70	−0.05	−0.15
↑ Contrast	100	0.75	0.94
↓ Contrast	100	−0.12	−0.35
↑ Saturation	100	0.12	0.16
↓ Saturation	100	−0.1	−0.13
↑ Redness	70	0.0003	0.0011
↓ Redness	60	−0.0003	−0.0010

where n represents the number of pixels in the image, I represents the set of all image coordinates, R_c represents a local receptive field centered on the coordinate c and max and min represent functions that compute the maximum and minimum values of their arguments respectively.

Table IV depicts parameter configurations that correspond to networks that have been optimized for five different functions. The functions from left to right are: decrease noise (↓ N), increase contrast (↑ C), decrease contrast (↓ C), increase saturation (↑ S) and decrease saturation (↓ S). The degrees and types of impacts of HCs in different solutions (from Table IV) are shown in Table V. The column "activity" denotes whether a particular HC type is being used (activity = 1) or not (activity = 0) by the solution. The column "impact" refers to the effect observed at the PR layer, after disconnecting an HC type (i.e. by setting the HC type's input and output weights to zero), in terms of activity differences. The measured effect consists of the average absolute difference between PR cells at the last iteration, resulting from disconnecting an HC type in one condition and not interfering with the network in the other. If the difference is larger than zero, then one can conclude that the HC type has an impact on the functioning of the network and thus on the processing of the image. The column "directness" refers to the type of effect exhibited by an HC type: "zero" denotes no impact, "one" denotes an indirect effect with information flow from the PR layer to the HC layer, "two" denotes an indirect effect with information flow from the HC layer to the PR layer and "three" denotes both direct and indirect effects. For the sake of clarity, note that in the case of an HC type with directness 2, information from the PR layer reaches the HC indirectly via other HCs thanks to gap junctions, and is then fed back to the PR layer directly.

Table VI depicts three different solutions capable of increasing contrast, which were optimized with the proportion of blue cones synapsing on HC_1 constrained to zero (notice that all $P_{10} = 0$). This echoes findings by [14] regarding the primate retina where the authors note that the dendrites of H3 cells seem to be devoid of connections with blue cones. Although not depicted, it should be noted that out of 6 optimization experiments conducted in this context, 4 returned parameter configurations identical to the third solution in Table VI, whereas solutions 1 and 2 were found only once. Table VII summarizes the degree and type of impact of HC types in three solutions that were optimized for increasing contrast with the above mentioned constraint (i.e. the blue proportion of HC1 fixed to zero).

Figures 5 and 6 demonstrate the effect of running multiple iterations of two different OPL networks to 10 different images. Figure 5 demonstrates the application of a contrast enhancing network whereas Fig. 6 shows the result of processing with a saturation enhancing network. Contrast and saturation measures of source images (before processing) are shown at iteration 0. Apart from the 10 curves representing each image, the graphs also depict averages for all curves. These results demonstrate the stability of the LRNN. They also show

TABLE IV
PARAMETERS OPTIMIZED FOR DIFFERENT FUNCTIONS.

Cell	Parameters		↓N	↑C	↓C	↑S	↓S
PR GJs	Light -> cone	P1	0.12	0.78	0.00	0.87	0.95
	Self	P2	0.84	0.53	0.00	0.32	1.00
	pos =; chrom ≠	P3	0.11	0.00	0.00	0.00	0.34
	pos ≠; chrom =	P4	0.44	0.03	0.00	0.05	0.00
	pos ≠; chrom ≠	P5	0.00	0.00	0.57	0.00	0.00
HC 1	in Rad	P6	0.17	0.57	0.00	1.00	0.27
	out Rad	P7	0.66	0.94	0.28	0.62	0.00
	Red	P8	0.28	0.68	0.62	0.63	0.92
	Green	P9	0.00	0.88	0.39	0.82	0.00
	Blue	P10	0.90	0.96	1.00	0.75	0.56
	PR-HC w	P11	0.33	0.50	0.84	0.21	0.00
	HC-PR w	P12	0.78	1.00	1.00	0.60	0.00
HC 2	in Rad	P13	0.42	0.00	0.13	0.41	0.00
	out Rad	P14	0.00	0.97	0.46	0.00	1.00
	Red	P15	0.16	0.35	0.45	0.36	0.89
	Green	P16	0.92	0.97	0.81	0.05	0.14
	Blue	P17	0.00	0.00	0.88	0.18	0.28
	PR-HC w	P18	0.05	1.00	0.63	0.00	0.77
	HC-PR w	P19	0.62	0.05	0.80	0.27	0.30
HC3	in Rad	P20	1.00	0.69	0.01	0.50	0.48
	out Rad	P21	1.00	0.17	0.39	0.17	0.00
	Red	P22	0.35	1.00	0.00	0.70	0.51
	Green	P23	1.00	0.68	0.83	0.45	0.00
	Blue	P24	0.06	0.45	0.82	0.59	0.00
	PR-HC w	P25	0.15	0.46	0.67	0.49	0.04
	HC-PR w	P26	0.74	1.00	0.91	0.68	0.00
HC GJs	Self	P27	0.94	0.55	1.00	1.00	0.94
	pos =; HC ≠	P28	1.00	0.00	1.00	0.34	0.00
	pos ≠; HC =	P29	0.97	0.37	0.08	0.00	0.27
	pos ≠; HC ≠	P30	0.10	0.69	0.00	1.00	0.53
	Num. Iter.	P31	0.95	0.08	0.50	0.46	0.07

TABLE V
THE DIRECTNESS AND IMPACT OF HC ACTIVITY.

		Activity	Impact	Directness
↓N	HC 1	1	109.6	3
	HC 2	1	109.6	1
	HC 3	1	74.4	3
↑C	HC 1	1	32.9	3
	HC 2	1	0.9	3
	HC 3	1	17.1	3
↓C	HC 1	1	116.3	3
	HC 2	1	116.3	3
	HC 3	1	116.3	3
↑S	HC 1	1	12.0	3
	HC 2	0	0.0	0
	HC 3	1	12.7	3
↓S	HC 1	0	0.0	0
	HC 2	1	2.3	3
	HC 3	0	0.0	0

TABLE VI
"BLUE ZERO" SOLUTIONS FOR ↑CONTRAST.

Cell	Parameters		Sol. 1	Sol. 2	Sol. 3
PR GJs	Light -> cone	P1	1.00	0.00	0.77
	Self	P2	1.00	1.00	0.17
	pos =; chrom ≠	P3	0.00	0.02	0.00
	pos ≠; chrom =	P4	0.00	0.04	0.03
	pos ≠; chrom ≠	P5	0.00	0.00	0.00
HC 1	in Rad	P6	0.79	1.00	0.91
	out Rad	P7	1.00	0.07	1.00
	Red	P8	0.96	1.00	0.85
	Green	P9	1.00	0.35	0.96
	Blue	P10	0.00	0.00	0.00
	PR-HC w	P11	1.00	1.00	0.53
	HC-PR w	P12	0.56	0.03	0.90
HC 2	in Rad	P13	0.08	0.88	0.63
	out Rad	P14	0.21	0.87	0.38
	Red	P15	0.38	1.00	0.33
	Green	P16	0.44	1.00	0.00
	Blue	P17	1.00	1.00	0.72
	PR-HC w	P18	0.58	0.55	0.26
	HC-PR w	P19	0.71	0.86	1.00
HC 3	in Rad	P20	0.98	0.02	0.01
	out Rad	P21	1.00	0.00	0.89
	Red	P22	0.17	1.00	0.06
	Green	P23	0.45	0.00	0.36
	Blue	P24	1.00	0.32	0.59
	PR-HC w	P25	1.00	0.27	1.00
	HC-PR w	P26	0.77	1.00	0.76
HC GJs	Self	P27	1.00	0.45	0.96
	pos =; HC ≠	P28	0.00	1.00	0.44
	pos ≠; HC =	P29	0.24	0.03	0.85
	pos ≠; HC ≠	P30	0.23	1.00	0.16
	Num. Iter.	P31	1.00	0.91	0.50

TABLE VII
HC IMPACTS FOR "HC1 ZERO BLUE" SOLUTIONS.

		Activity	Impact	Directness
Sol. 1	HC1	1	111.1	3
	HC2	1	111.1	3
	HC3	1	111.1	3
Sol. 2	HC1	1	110.3	1
	HC2	1	48.3	3
	HC3	1	110.3	1
Sol. 3	HC1	1	21.8	3
	HC2	1	12.2	3
	HC3	1	16.0	3

how image properties can be fine-tuned by applying multiple iterations. Notice how contrast curves are more variable and thus less predictable than saturation curves. Based on Fig. 6, if we know the saturation of a source image we should be able to predict the saturation of the corresponding processed image, after any number of OPL iterations.

Fine graded control of image properties (e.g. contrast) can be effected not only by applying multiple processing iterations but also by modulating specific parameters. Figures 7 and 8, demonstrate the modulation of parameters that exhibit both direct and inverse proportionalities to contrast respectively. The x-axis depicts different parameter settings in the range $[0, 1]$ whereas the y-axis depicts the contrast of the resulting processed image. In the case of Fig. 7, small 0.1 increments of the parameters 12 and 26 lead to mostly linear contrast increments. Notice how different parameters exhibit different

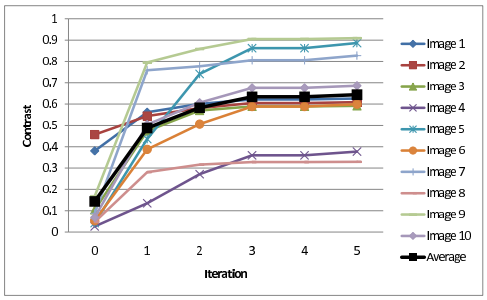

Fig. 5. Multiple iterations of contrast enhancement.

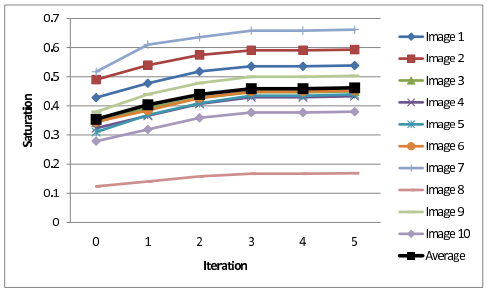

Fig. 6. Multiple iterations of saturation enhancement.

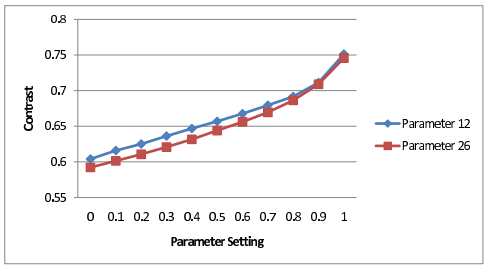

Fig. 7. Contrast parameters with direct proportionality.

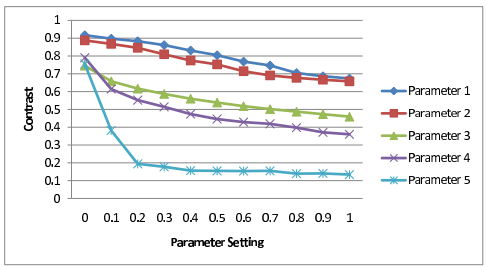

Fig. 8. Contrast parameters with inverse proportionality.

degrees of non-linearity and steepness in the way they are related to contrast.

Figure 9 depicts the relationship between parameters 12, 19, 29 and 30, and the level of *redness* in processed images. Recall that these parameters (HC to PR weights and HC gap junctions) do not correspond to rigid aspects of the network (e.g. connection patterns or dendritic tree radii) and therefore that their rapid modulation is indeed plausible. As with other cases of parameter modulation, the curves exhibit different types of proportionality (direct and inverse), and different

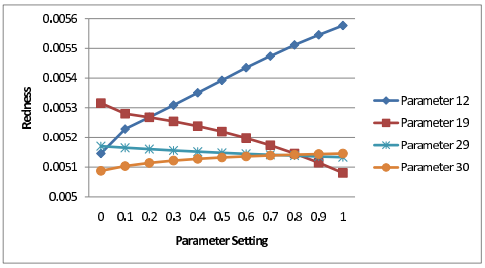

Fig. 9. Redness parameters.

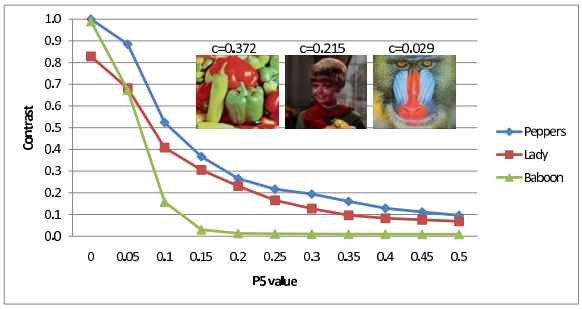

Fig. 10. Contrast control.

degrees of non-linearity and steepness.

Table VIII depicts the result of our search for a network configuration that would allow a single parameter to both decrease and increase the contrast of images. The configuration ("CC Sol") was obtained by initially optimizing the network for the increase of contrast ("iL (Contrast)"), subsequently fixing the parameter values for PR-HC RGB proportions, PR-HC input/output radii and PR-HC input/output weights, and subsequently optimizing the constrained network for the decrease of contrast. The resulting configuration suggested parameter P5 (i.e. inter-positional and inter-chromatic cone gap-junction) as a prime candidate for contrast control. This is also consistent with the results in Fig. 8.

The different curves in Figure 10 depict contrast levels for different images based on different P5 settings using the CC solution of Table VIII. Original (unprocessed) contrast levels are indicated at the top of each source image (i.e. Peppers=0.372, Lady=0.215 and Baboon=0.029). Comparing the contrast levels of the source images to those of the processed images (as a consequence of different P5 settings) we can easily see that the configuration "CC Sol" can indeed both increase and decrease the contrast of images. Figure 11 depicts the processing results for different P5 values when applied to the Peppers image. Each image in Fig. 11 corresponds to the processing output of a network based on the CC solution for a different P5 setting (depicted on top) and resulting in a different contrast level (depicted at the bottom).

TABLE VIII
CONTRAST CONTROL SOLUTION.

Cells	Param. Descrip.	ID	Solutions	
			iL (Contrast)	CC Sol
PR GJs	Light -> cone	P1	0.78	0.80
	Self	P2	0.53	0.00
	pos =; chrom ≠	P3	0.00	0.00
	pos ≠; chrom =	P4	0.03	0.00
	pos ≠; chrom ≠	P5	0.00	1.00
HC 1	in Rad	P6	0.57	0.57
	out Rad	P7	0.94	0.94
	Red	P8	0.68	0.68
	Green	P9	0.88	0.88
	Blue	P10	0.96	0.96
	PR-HC w	P11	0.50	0.50
	HC-PR w	P12	1.00	1.00
HC 2	in Rad	P13	0.00	0.00
	out Rad	P14	0.97	0.97
	Red	P15	0.35	0.35
	Green	P16	0.97	0.97
	Blue	P17	0.00	0.00
	PR-HC w	P18	1.00	1.00
	HC-PR w	P19	0.05	0.05
HC 3	in Rad	P20	0.69	0.69
	out Rad	P21	0.17	0.17
	Red	P22	1.00	1.00
	Green	P23	0.68	0.68
	Blue	P24	0.45	0.45
	PR-HC w	P25	0.46	0.46
	HC-PR w	P26	1.00	1.00
HC GJs	Self	P27	0.55	0.83
	pos =; HC ≠	P28	0.00	0.00
	pos ≠; HC =	P29	0.37	0.00
	pos ≠; HC ≠	P30	0.69	0.00
	Num. Iter.	P31	0.08	1.00

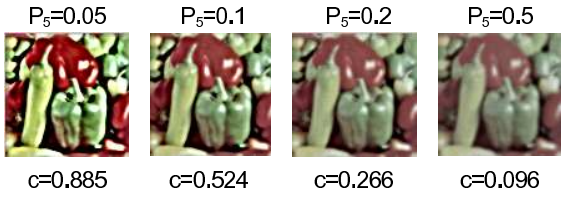

Fig. 11. Processing effects of different P5 values.

IV. DISCUSSION

A. Outer Retina Functions

The results section demonstrates that our simplified model of the outer retina is not only stable (see Figures 5 and 6) but is also functionally versatile. The fact that different configurations of the LRNN are capable of implementing the modulation of noise, brightness, contrast, saturation and even colour, suggests that the outer retina is at least in theory capable of implementing any one of these functions. Since some parameters control "rigid" (less adaptive) network features (e.g. dendritic tree radii and connectivity patterns), some solutions requiring specific values for these parameters may preclude other solutions. This mutual exclusivity is helpful in narrowing down the functions of the outer retina. Current knowledge seems to point to the fact that both luminance and contrast gain control [4] are implemented in the outer retina via independent mechanisms [8]. If other functions are also being

implemented (e.g. saturation and colour modulation) as our experiments suggest might be possible, this begs the question of how these functions might be combined and whether they are independent of the other mechanisms. In this paper we have confirmed and elaborated on a well-known characteristic of the outer-retina, which is its functional versatility, but we have not addressed several problems that remain open, e.g.: 1) which sets of functions work concurrently, 2) what function switching and modulation takes place, 3) what mechanisms underlie function switching and modulation. In order to address these problems from a computational perspective we need to incorporate further biological details (e.g. cell morphologies, relative cell densities and ionic currents) in our models and make more extensive use of neurophysiological validation data sets.

Not only is the OPL versatile in the types of functions that it can implement, each function also generalizes reasonably well. Recall Table III for a summary of the generalization capabilities of the network. The table shows us that not all functions generalize equally well. The strongest functions are ↓noise, ↑↓contrast and ↑↓saturation. The weakest functions are ↑↓brightness and colour correction. This in itself might serve as an indication of outer retina functions, i.e.: functions that generalize better are more likely to be biologically plausible. This argument, of course, should be accepted only cautiously, for at this point there is not enough evidence to conclude that the weakness of a function such as colour control is due to limitations of the model or constraints of the actual OPL. For example, the relatively lower accuracy of brightness control, is most probably because the mechanisms involved in luminance gain control are not represented in the model. The addition of new nonlinearities and mechanisms to the model might lead to both effective luminance control and possibly even adequate colour correction.

B. LRNN Parameters

This subsection will briefly describe the main relationships between specific parameter settings (e.g. Table IV) and different functions. To start with, notice how parameter P4 tends to be larger in the ↓noise solution. This is because of the averaging and therefore denoising effect of inter-positional (and in this case intra-chromatic) GJs. Notice how in the ↓noise solution, HC2 (i.e. the second HC type, counting from the top of the table) has a strong but indirect impact (refer to Table V). This horizontal cell, does receive input from the PR layer, but feeds back to it indirectly via other HC types (notice that the strength of GJs between HCs of different types at the same position is 1.0 and at different positions is 0.1).

For the ↓saturation solution, parameter P3 is relatively strong because it represents the strength of intra-positional and inter-chromatic GJs. The effect of an inter-chromatic GJ is to attract colours towards more central (grayer) values, which is the intended result of decreasing saturation. Tests pertaining to the degree of impact of different HC types on the PR layer confirmed that in the ↓saturation solution only HC2 had an impact (refer to Table V).

With regards to the ↑saturation solution first of all notice how P3 is set to zero, since this is an inter-chromatic GJ that leads to desaturation. Secondly, notice how HC2 has no impact on the PR layer (refer to Table V) and how the remaining HCs exhibit different dendritic radii (one small and one large) and different proportions of connections with cones of different wavelength (the order of spectral proportions in one HC is the reverse of the order in the other HC). Finally, notice how the strength of inter-positional GJs is $zero$ for HCs of the same type but one for HCs of different types.

Notice how in the ↓noise solution parameter P3 is non-zero. This means that there is a desaturating force (due to interchromatic GJs), which on the surface appears to be inconsistent with denoising, since the latter function should preserve the colour properties of images. The reason why there is no inconsistency is that the rest of the circuit (i.e. PR-HC connectivity) is wired similarly to the ↑saturation solution. Notice how all HCs in the ↓noise solution have an impact on the PR layer (refer to Table V). The existence of this circuit means that there is a saturating force counteracting the effects of parameter P3. This is likely to be a general strategy adopted by biological systems. Since P3 represents the strength of GJs between cones of different wavelengths but equivalent positions, this strategy (counteracting desaturation via the PR-HC circuit) allows for denoising without a blurring effect across neighbors of different spatial coordinates. Of course, the more cones that are present for each spatial coordinate, the more effective this strategy is. This co-existence of multiple functions (in this case ↓noise, ↓saturation and ↑saturation) appears to be a common design principle in many biological neural systems, and is very closely related to the concept of Polymorphic Networks [31] [32] [33]. The strategy raises important questions regarding the evolutionary pressures for compact multi-function retinal architectures and the independent modulation of component functions, the understanding of which may be partly provided by the framework of control theory [34] [35]. The fact that this *denoising and resaturating* micro-circuit emerged from our GSO without any manual intervention suggests that this is a natural strategy whose existence in biological retinae deserves to be verified.

The ↑contrast solution is quite similar to the ↑saturation solution. Table V shows that all HCs in this solution have an impact on the PR layer, although HC2 has a relatively weak effect. HC1 and HC3, as in the ↑saturation solution, exhibit distinct dendritic radii and inverse chromatic proportions of PR-HC connections. The input/output weights for both HC1 and HC3 are approximately $0.5/1.0$. Notice that although the parameter settings for HC GJs are quite distinct for both the ↑contrast and ↑saturation solutions, no functional conclusions can be drawn from this because both solutions involve only a single iteration (see P31), which means that the GJ effects on the PR layer will not be observed, since they only manifest in the second iteration (in the first iteration they only affect HCs). In other words, for solutions involving single iterations, any HC GJ configuration can be used, with no consequence to the image extracted from the PR layer.

The main differences between the ↑contrast and ↑saturation solutions include: 1) different HC1/HC3 PR-impact ratios, 2) different RGB proportion orders (e.g. RGB-GBR vs. RBG-GBR), 3) the impact of HC2 and 4) radii properties (e.g. the ratio of input/output radii is the same for HC3 but the reverse for HC1).

The solution for decreasing contrast seems to be the result of parameters P1, P2, P3 and P4 all being zero. Interestingly all HCs had strong impacts on the PR layer (Table V).

C. Direct and Indirect HCs

Optimization generally reveals hard to anticipate solutions, and the configurations described above are no exception. One noteworthy example of this was the unexpected emergence of HCs adopting indirect strategies of interaction with the PR layer. If a HC does not receive input directly from the PR (because, for example, the HC's input weight is zero), it can still receive indirect input via other HCs thanks to GJs. Also, if a HC does not directly influence the PR layer (because, for example, the HC's output weight is zero), it may still indirectly do so by influencing neighboring HCs (with direct influence on the PR layer) via GJs. For examples of solutions with indirect HC types refer to the ↓noise solution in Table V and solution 2 in Table VII. These results demonstrate that HCs with either no direct input or no direct output from/to the PR layer, can still have a strong impact on the latter. Questions that require further investigation pertain to what unique advantages are afforded by indirect HC types, and in what circumstances are they required?

D. Modulation

A fundamental question pertains to how putative visual functions implemented by the outer retina can be controlled (or modulated) in real-time (see [36] for an application of neural networks to the real-time solving of linear inequality systems). Rigid parameters such as HC radii and connectivity patterns are not suitable candidates for modulation due to the real-time requirement. However, parameters governing GJ strengths, cell sensitivities and connection weights, are all valid candidates. Figure 7 demonstrates that it is possible to increase or decrease contrast by modulating the weights of connections between HCs and PRs. Another possibility is to vary the number of iterations involved in processing. Figure 5 demonstrates how the degree of contrast enhancement obtained is directly proportional to the number of iterations applied. This multi-iteration effect might be realizable biologically by changing the speed and latency of cell responses. Ultimately, we would like to minimize the number of parameters required to modulate whilst maximizing the degree of control exercised. Ideally we would like a small set of parameters to select different functions (e.g. colour correction), and activate it to different degrees (e.g. large gradations) and in different ways (e.g. remove blue illuminant). The current paper provides early (modest) steps towards this goal.

E. Biological Questions

1) Contrast Gain Control: An important question in many Neuroscience related fields concerns the neural substrates of contrast gain control (CGC). Related to CGC are the concepts of contrast sensitivity, estimation, enhancement, attenuation and adaptation. Although initially it was believed that CGC was implemented at the level of the cortex, today we have ample evidence showing us that the phenomenon can be found as early as the retina. Both retinal ganglion cells (RGCs) and bipolar cells (BCs) [4] have been shown to exhibit CGC. Since we are here more concerned with the OPL, we will focus on CGC at the level of BCs. To date there is no concrete consensus on the mechanisms that underlie bipolar-cell contrast gain control (BC-CGC).

Our experiments (see Table VIII and Figures 10 and 11) suggest that BC CGC may be primarily implemented via PR-HC circuitry and PR (and possibly HC) GJs. Note that the possibility that HCs may implement CGC does not imply that these cells should also exhibit the phenomenon themselves (the experimental evidence in [4] suggests that mammalian HCs do not show signs of CGC). We suggest that the "rigid" parameters of our OPL model (i.e. connectivity and diameters of dendritic fields) are optimized for enhancing contrast and that the adaptive parameters (e.g. gap junctions) are used for putting breaks on the enhancement. By modulating relevant gap-junctions (e.g. parameter P5) the retina can either increase ("less breaks") or decrease ("more breaks") contrast depending on the statistics of the scene.

Note that what we are proposing here is a simple and plausible mechanism for both increasing and decreasing contrast. We have not proposed any mechanism for estimating contrast (explicitly or implicitly). In others words, even though we suggest that contrast modulation may be mediated via the modulation of inter-positional and inter-chromatic PR GJs, we have not outlined what may control these GJs.

2) HC Types and Connectivity: Our results are not yet sufficient for resolving the debate concerning the number of primate HC types, however the fact that most optimized solutions exhibited three active HC types (Table VII) suggests that evolution might favour this possibility. Having said this, the results also show that solutions with two HC types (Table V) are also capable of implementing visual functions such as contrast control. Note that we have deliberately avoided discussing the axonic connections of the primate horizontal cell H1, since they involve rod-HC connections, which fall out of the scope of this paper. Only one of our optimized solutions (i.e. ↓saturation) exhibited a configuration involving a single active HC type.

With regards to the spectral specificity of PR-HC connections, our optimization experiments reveal that for all visual functions investigated, and in particular contrast control, the most likely configurations involve different proportions of connections between cones of different wavelengths and different HC types. In all the experiments conducted, no solution emerged naturally whereby the proportions of red,

green and blue cone connections were the same within each HC type. Refer for example to Table VI. Although this does not constitute incontrovertible evidence that primate cones and HCs are connected in a spectrally specific way, it does suggest that this is the most natural (likely) solution from the functional (e.g. contrast control) point of view. Whether this argument still holds if we consider developmental constraints is an important question which we intend to pursue in future work.

ACKNOWLEDGMENT

The authors would like to thank the anonymous reviewers for their very helpful comments and suggestions.

REFERENCES

[1] T.H. Maul, A. Bargiela and L.J. Ren, "A Neuroalgorithmic Investigation of the Outer Retina," in the European Conference on Modelling and Simulation, June 2010.
[2] H. Kolb, E. Fernandez, J. Schouten, P. Ahnelt, K.A. Linberg, and S.K. Fisher, "Are there three types of horizontal cell in the human retina?", Journal of Comparative Neurology, 343:3, pp. 370–386, 1994.
[3] D.M. Dacey, and B.B. Lee, D.K. Stafford, J. Pokorny, and V.C. Smith, "Horizontal cells of the primate retina: cone specificity without spectral opponency", AAAS, 271:5249, 1996.
[4] D.L. Beaudoin, B.G. Borghuis, and J.B. Demb, "Cellular basis for contrast gain control over the receptive field center of mammalian retinal ganglion cells", Journal of Neuroscience, 27:10, 2007.
[5] G.D. Field, and E.J. Chichilnisky, "Information processing in the primate retina: circuitry and coding", Annual Reviews, 30, pp. 1–30, 2007.
[6] M. Egmont-Petersen, D. De Ridder, and H. Handels, "Image processing with neural networks – a review", Pattern Recognition, 35:10, pp. 2279–2301, 2002.
[7] R.H. Masland, "The fundamental plan of the retina", Nature Neuroscience, 4, pp. 877–886, 2001.
[8] V. Mante, R.A. Frazor, V. Bonin, W.S. Geisler, and M. Carandini, "Independence of luminance and contrast in natural scenes and in the early visual system", Nature Neuroscience, 8:12, pp. 1690–1697, 2005.
[9] D. Dacey, O.S. Packer, L. Diller, D. Brainard, B. Peterson, and B. Lee, "Center surround receptive field structure of cone bipolar cells in primate retina", Vision Research, 40:14, pp. 1801–1811, 2000.
[10] D.M. Dacey, "Parallel pathways for spectral coding in primate retina", Annual Review of Neuroscience, 23:1, pp. 743–775, 2000.
[11] H. Wassle, B.B. Boycott, and J. Rohrenbeck, "Horizontal cells in the monkey retina: cone connections and dendritic network", European Journal of Neuroscience, 1:5, pp. 421–435, 2006.
[12] A. Szel, T. Diamanstein, and P. Röhlich, "Identification of the blue-sensitive cones in the mammalian retina by anti-visual pigment antibody", The Journal of Comparative Neurology, 273:4, pp. 593–602, 2004.
[13] M.B. Shapiro, S.J. Schein, and F.M. De Monasterio, "Regularity and structure of the spatial pattern of blue cones of macaque retina", Journal of the American Statistical Association, 80:392, pp. 803–812, 1985.
[14] P. Ahnelt, and H. Kolb, "Horizontal cells and cone photoreceptors in primate retina: a Golgi-light microscopic study of spectral connectivity", The Journal of Comparative Neurology, 343:3, pp. 387–405, 2004.
[15] B.B. Boycott, L. Peichl, and H. Wassle, "Morphological types of horizontal cell in the retina of the domestic cat", Proceedings of the Royal Society of London. Series B, Biological Sciences, 203:1152, 229–245, 1978.
[16] H. Wassle, D.M. Dacey, T. Haun, S. Haverkamp, U. Grunert, and B.B. Boycott, "The mosaic of horizontal cells in the macaque monkey retina: with a comment on biplexiform ganglion cells" Visual Neuroscience, 17:4, pp. 591-608, 2000.
[17] H. Kolb, A. Mariani, and A. Gallego, "A second type of horizontal cell in the monkey retina" Journal of Comparative Neurology, 189, pp. 31-44, 1980.
[18] A. Wohrer, P. Kornprobst, and T. Vieville, "From light to spikes: A large-scale retina simulator", Proceedings of the IJCNN 2006, pp. 8995–9003, 2006.
[19] M. Ebner, "Evolving color constancy", Pattern Recognition Letters, 27:11, pp. 1220–1229, 2006.
[20] K.A. Zaghloul, and K. Boahen, "A silicon retina", Journal of Neural Engineering, 3, pp. 257–267, 2006.
[21] J.H. van Hateren, "A model of spatiotemporal signal processing by primate cones and horizontal cells", Journal of Vision, 7:3, 2007.
[22] V.C. Smith, J. Pokorny, B.B. Lee, and D.M. Dacey, "Sequential processing in vision: The interaction of sensitivity regulation and temporal dynamics", Vision Research, 48:26, pp. 2649–2656, 2008.
[23] R.G. Smith, "Simulation of an anatomically defined local circuit: the cone-horizontal cell network in cat retina", Visual Neuroscience, 12:03, pp. 545–561, 1995.
[24] S. Haykin, S. "Neural networks: a comprehensive foundation", Prentice Hall, 2008.
[25] E. Schutter, "Computational Modeling Methods for Neuroscientists", The MIT Press, 2009.
[26] R. Storn, and K. Price, "Differential evolution–a simple and efficient heuristic for global optimization over continuous spaces", Journal of Global Optimization, 11:4, pp. 341–359, 1997.
[27] D.E. Goldberg, "Genetic Algorithms in Search and Optimization", Addison-Wesley, 1989.
[28] B. Tessema, and G.G. Yen, "An adaptive penalty formulation for constrained evolutionary optimization", Systems, Man and Cybernetics, Part A: Systems and Humans, IEEE Transactions on, 39:3, pp. 565–578, 2009.
[29] C. Liu, W.T. Freeman, R. Szeliski, and S.B. Kang, "Noise estimation from a single image," 2006 IEEE Computer Society Conference on Computer Vision and Pattern Recognition, 1, 2006.
[30] R. Highnam, and J.M. Brady, "Mammographic Image Analysis (Computational Imaging and Vision," Springer, 1999.
[31] E. Marder, "Polymorphic neural networks," Current Biology, 4, pp. 752–754, 1994.
[32] R.M. Harris-Warrick, and E. Marder, "Modulation of neural networks for behavior," Annual Review of Neuroscience, 14:1, pp. 39–57, 1991.
[33] Y. Makino, M. Akiyama, and M. Yano, "Emergent mechanisms in multiple pattern generation of the lobster pyloric network," Biological Cybernetics, 82:6, pp. 443–454, 2000.
[34] A. Roy, "Connectionism, controllers, and a brain theory," Systems, Man and Cybernetics, Part A: Systems and Humans, IEEE Transactions on, 38:6, pp. 1434–1441, 2008.
[35] H. Zhang, M. Li, J. Yang, and D. Yang, "Fuzzy model-based robust networked control for a class of nonlinear systems," Systems, Man and Cybernetics, Part A: Systems and Humans, IEEE Transactions on, 39:2, pp. 437–447, 2009.
[36] A. Cichocki and A. Bargiela, "Neural Networks for Solving Linear Inequality Systems," Parallel Computing, 22:11, pp. 1455–1475, 1997.

Tomás H. Maul received a B.Sc. (Hons.) degree in Biological Psychology from the University of St. Andrews, an M.S. degree in Computer Science at Imperial College and a Ph.D. degree in Computational Neuroscience at the University of Malaya. He worked for two years at MIMOS Bhd. as a Senior Researcher in the fields of Pattern Recognition and Computer Vision. He is currently an Assistant Professor at the University of Nottingham Malaysia Campus, where he conducts research in the areas of Neural Computation and Computer Vision.

Andrzej Bargiela is Professor and Director of Computer Science at the University of Nottingham, Malaysia Campus. He is a member of the Automated Scheduling and Planning research group in the School of Computer Science at the University of Nottingham. Since 1978 he has pursued research focused on processing of uncertainty in the context of modelling and simulation of various physical and engineering systems. His current research falls under the general heading of Computational Intelligence and involves mathematical modelling, information abstraction, parallel computing, artificial intelligence, fuzzy sets and neurocomputing.

Lee Jung Ren is currently pursuing his PhD in Computer Science at The University of Nottingham, Malaysia Campus. He did a Bachelors of Computer Science in the same university in 2007 where he developed a Medical Diagnosis Aiding application with Semantic Web for his Final Year Dissertation. His current research is focused on a neuroalgorithmic approach to retinal modeling.